InGaAsP avalanche photodetectors for non-gated 1.06 μm photon-counting receivers

Mark A. Itzler*, Xudong Jiang, Rafael Ben-Michael, Krystyna Slomkowski
Princeton Lightwave Inc., 2555 US Route 130 South, Cranbury, NJ 08512

Michael A. Krainak, Stewart Wu, Xiaoli Sun
NASA Goddard Space Flight Center, Mail Code 554, Building 19, Greenbelt, MD 20771

ABSTRACT

For the detection of single photons at 1.06 μm, silicon-based single photon avalanche diodes (SPADs) used at shorter wavelengths have very low single photon detection efficiency (~1 – 2%), while InP/InGaAs SPADs designed for telecommunications wavelengths near 1.5 μm exhibit dark count rates that generally inhibit non-gated (free-running) operation. To bridge this "single photon detection gap" for wavelengths just beyond 1 μm, we have developed high performance, large area (80 – 200 μm diameter) InP-based InGaAsP quaternary absorber SPADs optimized for operation at 1.06 μm. We demonstrate dark count rates that are sufficiently low to allow for non-gated operation while achieving detection efficiencies far surpassing those found for Si SPADs. At a detection efficiency of 10%, 80 μm diameter devices exhibit dark count rates below 1000 Hz and photon counting rates exceeding 1 MHz when operated at -40 °C.

Keywords: avalanche photodiodes, single photon detector, SPAD, InGaAsP, 1.06 micron

1. INTRODUCTION

The efficient detection of single photons at 1.06 μm is of considerable interest for lidar/ladar systems designed for remote sensing and ranging [1] as well as for free-space optical transmission in photon-starved applications [2]. However, silicon-based single photon avalanche diodes (SPADs) used at shorter wavelengths have very low single photon detection efficiency (~1 – 2%) at 1.06 μm, while InP/InGaAs SPADs designed for telecommunications wavelengths near 1.5 μm exhibit dark count rates that generally inhibit non-gated (free-running) operation. To bridge this "single photon detection gap" for wavelengths just beyond 1 μm, we have developed high performance, large area (80 – 200 μm diameter) InP-based InGaAsP quaternary absorber SPADs optimized for operation at 1.06 μm and based on a highly reliable planar geometry avalanche photodiode structure.

When an avalanche photodetector is biased above its breakdown voltage, the creation of a single electrical carrier can induce a run-away avalanche that gives rise to a detectable macroscopic current. In this mode of operation, often referred to as Geiger mode, the detector is sensitive to the absorption of a single photon. Our 1.06 μm SPAD device design shares similarities with InP/InGaAs SPAD designs we have employed for longer wavelength operation with a 1.65 μm cutoff [3]. Related mesa-geometry small-area devices have been studied by researchers at MIT-Lincoln Labs [4,5] for use in ladar imaging arrays.

In this paper, we demonstrate large area 1.06 μm SPADs with dark count rates sufficiently low to allow for non-gated operation that achieve detection efficiencies far surpassing those found for Si SPADs at this wavelength. At a detection efficiency of 10%, 80 μm diameter devices exhibit dark count rates below 1000 Hz and photon counting rates exceeding 1 MHz when operated at -40 °C. Significantly higher detection efficiencies (30 – 50%) are achievable with acceptable tradeoffs in dark count rate. We also present detailed modeling for the dependence of dark count rate on detection efficiency at various temperatures and demonstrate excellent agreement with experimental results. We then compare the behavior of 1.06 μm SPADs with longer wavelength (~1.5 μm) InP-based InGaAs ternary absorber SPADs fabricated on a related device design platform. Finally, we present an initial characterization of afterpulsing effects in the 1.06 μm SPADs.

*mitzler@princetonlightwave.com; tel: 1 609 495 2551; www.princetonlightwave.com

Enabling Photonics Technologies for Defense, Security, and Aerospace Applications III, edited by M.J. Hayduk, A.R. Pirich, P.J. Delfyett Jr., E.J. Donkor, J.P. Barrios, R.J. Bussjager, M.L. Fanto, R.L. Kaminski, G.Li, H.Mohseni, E.W. Taylor, Proc. of SPIE Vol. 6572, 65720G, (2007) · 0277-786X/07/$18 · doi: 10.1117/12.719471

2. SPAD DEVICE DESIGN

By virtue of the photoelectric effect, positive-intrinsic-negative (PIN) photodetectors based on the InP-lattice-matched InGaAsP material system can efficiently detect light in the short-wavelength infrared range from 1.0 – 1.7 µm. However, their responsivity is quantum-limited to, at best, one electron-hole pair generated per input photon. Avalanche photodetectors benefit from internal gain due to a process known as impact ionization that leads to multiple electron-hole pairs per input photon. Applying a larger reverse voltage to the avalanche detector will result in a larger gain, until the breakdown voltage V_{br} is reached. For bias voltages larger than V_{br}, the electron-hole generation process can become self-sustaining and result in an avalanche of charge limited only by external circuit resistance.

2.1 General SPAD operation

Traditional optical receivers make use of linear mode avalanche photodiodes (APDs), for which the output photocurrent is linearly proportional to the intensity of the optical input. Internal APD gain can provide significant improvement in high-bandwidth optical receiver sensitivity. In contrast to linear mode operation below V_{br}, if an avalanche photodetector is biased above V_{br}, then a single photoexcited carrier can induce a run-away avalanche that gives rise to an easily detectable macroscopic current. In this case, the detector is sensitive to a single photon input and is referred to as a single photon avalanche diode (SPAD). This mode of operation is often referred to as 'Geiger mode' because of its similarity to Geiger-Muller detectors, in which particle emission from radioactive materials gives rise to an avalanche of carriers from ionized gas atoms.

Linear mode APD performance has a noise floor determined by the shot noise associated with leakage current, or dark current, that exists in the absence of input photons. Analogously, SPAD performance is degraded by false counts, or dark counts, that arise when carriers are created by processes other than photoexcitation. Both thermal excitation and field-mediated creation of free carriers (i.e., tunneling processes) contribute to the dark count rate (DCR). To improve the performance of SPADs in the presence of significant DCR, they are often operated in gated mode. The detector is biased at a baseline voltage just below the breakdown voltage, and to 'arm' the detector, a gate pulse is applied to bring the detector bias above breakdown for a short period of time, generally between 1 and 100 ns. For applications in which the photon arrival time is sufficiently well-known, a shorter gate pulse can be used to reduce the likelihood of a dark count being generated within the gate. However, for applications in which photon arrival times are not deterministic, the preferred operating mode is non-gated, or free-running, in which the detector is armed continuously.

Once an avalanche is initiated, it must be quenched. Gated quenching allows the avalanche to persist until the bias is reduced below V_{br} according to the fixed gate duration. For non-gated operation, there are two primary quenching techniques. Passive quenching employs a resistor in series with the APD so that the avalanche current induces a voltage across the resistor and drops the APD bias below V_{br}. Although this drop can be rapid, passive quenching often entails a rather long 'reset' time dictated by the product of the quench resistance R and the detector capacitance C. Active quenching uses circuitry to force the APD bias below V_{br} once an avalanche is detected and then to actively reset the detector to its armed state in a time much shorter than the reset time corresponding to the passive quench RC time constant.

2.2 1.06 µm SPAD device structure

All InP-based avalanche photodetectors deployed today are based on the separate absorption and multiplication (SAM) regions structure [6]. In Figure 1, we present a schematic representation of our basic 1.06 µm device design platform. This design entails a quaternary InGaAsP layer (E_g ~ 1.03 eV), lattice-matched to InP, chosen to efficiently absorb photons at the wavelength of interest (i.e., 1.06 µm). This absorption layer is spatially separated from a wider bandgap InP region (E_g ~ 1.35 eV) in which avalanche multiplication occurs. A primary goal of the design is to maintain low electric field in the narrower bandgap absorber (to avoid dark carriers due to tunneling) while maintaining sufficiently high electric field in the multiplication region (so that impact ionization leads to significant avalanche multiplication). The inclusion of a charged layer between the absorption and multiplication regions (the SACM structure [7]) allows for more flexible tailoring of the internal electric field profile, along with the associated avalanche process, and is common to many InP-based avalanche diodes used today. Grading layers between the InGaAsP and InP layers are added to mitigate carrier (specifically hole) trapping effects that result from the valence band offset that arises in an abrupt heterojunction of InGaAsP and InP [8].

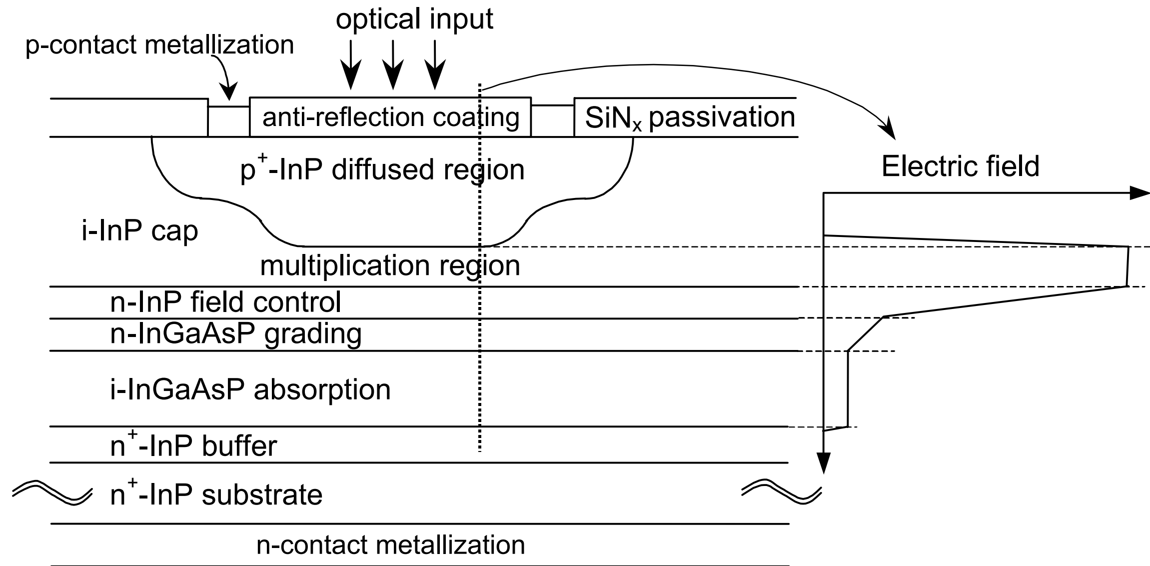

Figure 1. Schematic representation of 1.06 μm SPAD design platform.

The lateral structure of our design employs a buried p-n junction to guarantee edge breakdown suppression, low perimeter leakage, and high reliability. The device active area geometry is determined by the patterning of a SiN dielectric passivation layer to create a diffusion mask. A subsequent diffusion of Zn dopant atoms creates a p^+-InP region within the i-InP cap layer. The quasi-cylindrical junction that is formed by a single diffusion exhibits electric field enhancement where the junction curvature is maximum and leads to premature avalanche breakdown at the edges of the device. To suppress this edge breakdown phenomenon, we use two diffusions to tailor the junction profile [9] so that the junction is deeper in the central part of the active area than it is in the junction periphery. This design ensures that the gain profile across the center part of the active region is uniform and that the gain is reduced in the peripheral region of the device. With this buried junction design, the formation of a high-quality SiN passivation layer can guarantee low perimeter leakage and extremely stable long-life performance. The use of this platform for the fabrication of linear mode APDs is described further in references [10] – [12].

3. FREE-RUNNING PHOTON COUNTING MEASUREMENTS

Free-running photon counting data were obtained using a Poisson source of 1.06 μm photons, the SPAD detector, and appropriate backend electronics. We used a commercially available active quenching circuit (AQC) described in [13], and photon flux was calibrated using a reference Si-based SPAD detector. Total count rate was measured as a function of incident photon flux, and photon flux was swept over a very wide range from 10^{-1} to 10^{8} photons per second. We note that, to our knowledge, this measurement technique has not been reported previously in the photon counting literature.

3.1 Dark count rate vs. detection efficiency dependence extracted from count rate vs. photon flux

The data in Figure 2 were obtained by measuring the total count rate at 230 K from the SPAD-AQC detector as a function of photon flux for an 80 μm diameter active area SPAD. The constant (flux-independent) count rate for low photon fluxes ($< 10^3$ s^{-1}) is due to dark counts. For flux values larger than $\sim 10^4$ s^{-1}, the count rate increases approximately linearly with photon flux, indicating single photon counting with a dynamic range of three orders of magnitude in photon flux. For the higher bias data sets, corresponding to dark count rates larger than $\sim 10^2$ s^{-1}, count rates at photon flux values beyond $\sim 10^8$ s^{-1} saturate at rates on the order of a few MHz.

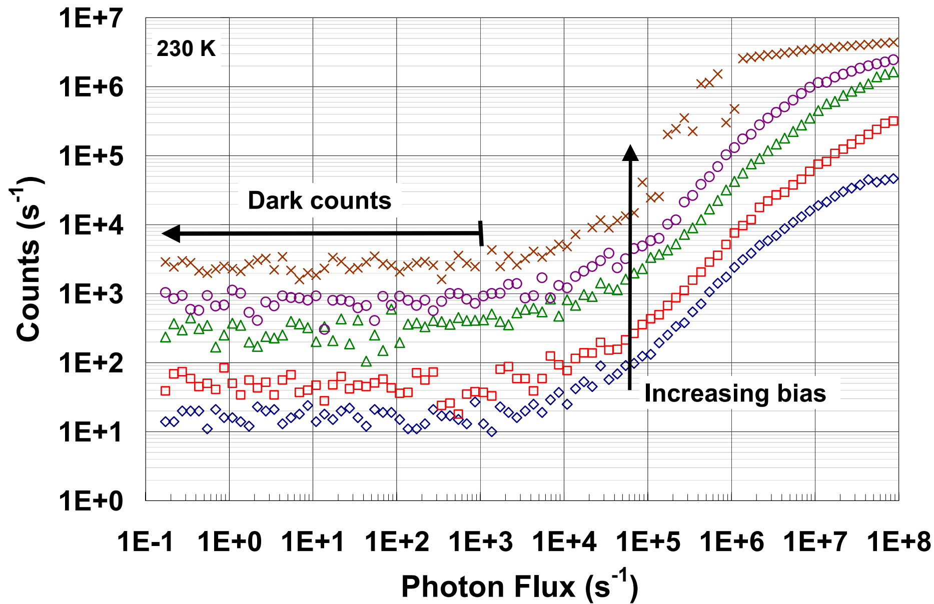

Figure 2. Free-running counts per second as a function of photon flux at 1064 nm for an 80 μm diameter InGaAsP/InP SPAD at 230 K for five different bias voltages using an active quenching circuit.

The detection efficiency (DE) can be computed using $(C_{tot} – C_d)/\Phi$, where C_{tot} is the total count rate, C_d is the dark count rate, and Φ is the photon flux. Using C_{tot} at a photon flux value of $\Phi \sim 10^6$ s^{-1}, we calculate the 230 K dependence of DCR on DE, as shown by the open circles ('○') in Figure 3. (For the highest count rate dataset in Figure 2, indicated by 'x', we used $\Phi \sim 10^5$ s^{-1} since data at higher fluxes were noisy.) Similar data were obtained for 270 K and 295 K operation, indicated in Figure 3, with higher temperatures leading to higher DCR values.

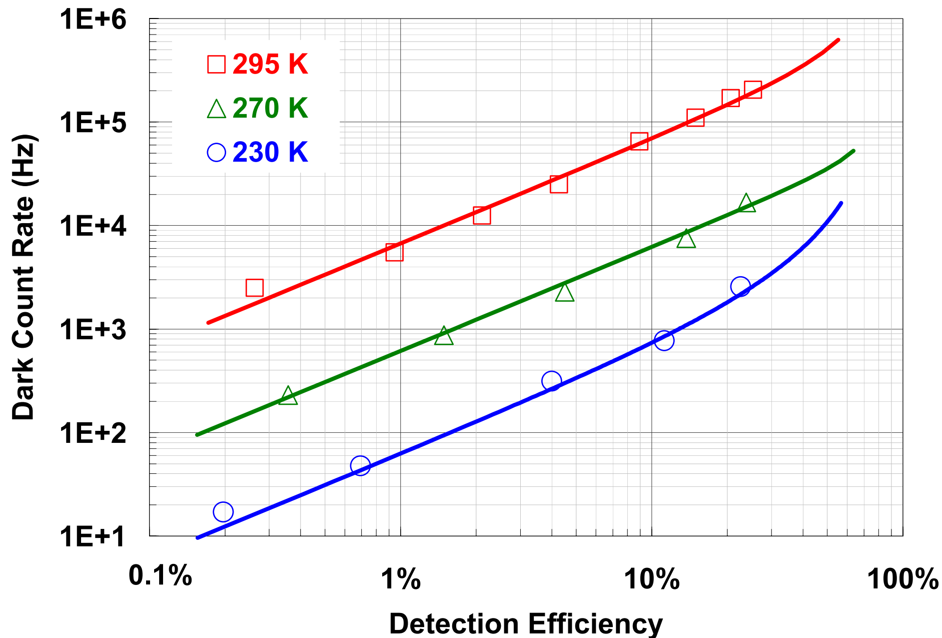

Figure 3. Dark count rate vs. detection efficiency for an InGaAsP/InP SPAD at 1064 nm. Experimental data at 295 K (squares), 270 K (triangles), and 230 K (circles) were extracted from count rate vs. photon flux measurements (as presented in Figure 2 for 230 K data). The solid lines are simulated performance; see Section 4 for discussion.

We have also carried out preliminary DCR vs. DE measurements of 1064 nm SPADs using a short (1 ns) gating technique with a gate frequency of 500 kHz that has been previously reported in the single photon counting literature [14],[15]. These initial gated-quenching results yield DCR vs. DE behavior that agrees reasonably well with the low temperature (230 K) results presented in Figure 3. One difference in these measurements is that the apparent overbias values ΔV used in the free-running measurements are markedly lower than the ΔV values used for the gated-mode characterization, which were consistent with typical values reported in the literature (e.g., DE ~ 20% achieved with ΔV~ 1 – 2 V). This discrepancy is being investigated.

3.2 Comparison of 1.06 µm SPAD results and 1.55 µm SPAD results

We have previously designed and fabricated 1.55 µm SPADs [3] on a design platform similar to that shown schematically in Figure 1 and described in Sub-section 2.2. This structure included an absorption layer consisting of $In_{0.53}Ga_{0.47}As$ (lattice-matched to InP), providing a long wavelength cut-off of ~1.65 µm. Measurements of the free-running count rate vs. photon flux on these 1550 nm SPADs provided data sets similar to those exhibited in Figure 2, but with substantially higher DCR. Performance modeling (summarized below) confirms that much higher DCR is expected for the 1550 nm structures due to thermal carrier generation in the small bandgap (E_g ~ 0.75 eV) InGaAs absorption layer. It is important to point out that the much larger DCR for the 1.55 µm structures—two to three orders of magnitude, depending on the temperature—greatly reduces the dynamic range in photon flux available for single photon detection at even modest detection efficiency values (e.g., 10%). Whereas the count rate vs. photon flux data for the 1064 nm device (see Figure 2) show that 10% detection efficiency can be realized for approximately three orders of magnitude in photon flux (from $\Phi \sim 10^4$ s^{-1} to $\Phi \sim 10^7$ s^{-1}), 10% detection efficiency on the 1550 nm SPAD is possible for less than one order of magnitude of photon flux, even at an operating temperature of 200 K.

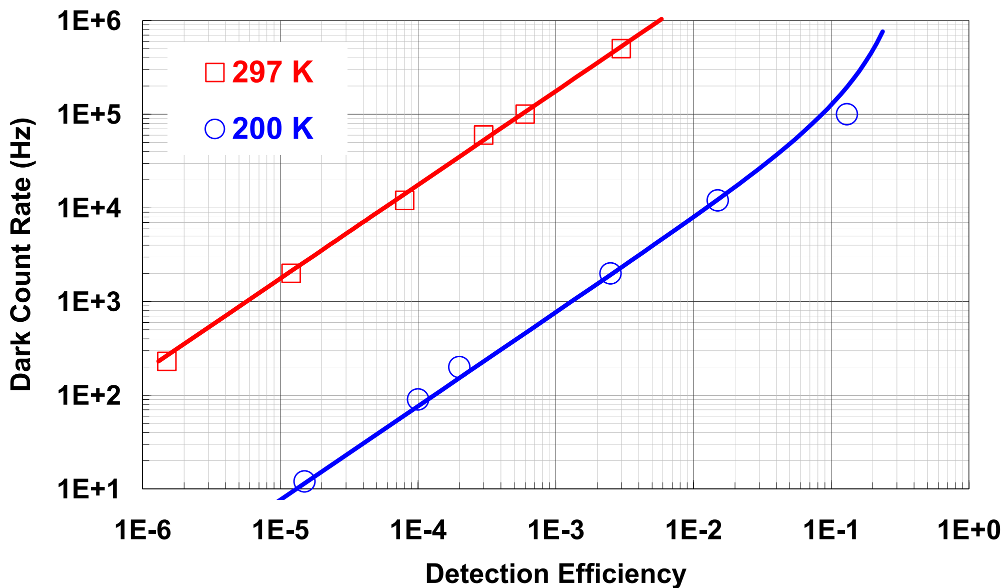

Figure 4. Dark count rate vs. detection efficiency for a 125 µm diameter InGaAs/InP SPAD at 1.55 µm. Experimental data at 297 K (squares) and 200 K (circles) were extracted from count rate vs photon flux measurements (similar to data in Figure 2 for 1.06 µm SPAD). The solid lines are simulated performance; see Section 4 for discussion.

4. THEORETICAL MODELING: DARK COUNT RATE VS. DETECTION EFFICIENCY

To obtain a better understanding of the DCR vs. DE behavior of our SPADs, we have performed theoretical modeling of the Geiger mode performance of these devices. Following the formalism of Donnelly, *et al.* [5], avalanche probabilities are calculated using field-dependent ionization coefficients. Non-local effects are neglected, as is valid for multiplication layer thicknesses ~1 µm and larger. Dark carrier generation is considered for all layers in the structure and includes temperature-dependent models for generation-recombination, band-to-band tunneling, and trap-assisted tunneling mechanisms. Details of our modeling are described in the remainder of this Section.

4.1 Computational model for dark count rate and detection efficiency

There are a number of mechanisms that generate carriers in a SPAD structure, including (i) thermally-generated or tunneling-generated bulk dark carriers and (ii) background- or signal-photon-generated photocarriers. In Geiger mode operation, these carriers have a bias-dependent finite probability P_a (generally less than 1) of initiating an avalanche if they reach the multiplication region.

The thermal generation rate per unit volume N_{th} is determined principally by Shockley-Read-Hall (SRH) processes and can be expressed as

$$N_{th} = \frac{n_i}{\tau_{SRH}} \tag{1}$$

where n_i is the intrinsic carrier concentration and τ_{SRH} is the lifetime related to SRH processes. Tunneling processes include direct band-to-band tunneling (BBT) and trap-assisted tunneling (TAT). The dark carrier generation rate per unit volume due to BBT can be expressed as [16]

$$N_{BBT} = \sqrt{\frac{2m_r}{E_g}}\frac{q^2F^2}{4\pi^3\hbar^2}\exp\left(-\frac{\pi\sqrt{m_r E_g^3}}{2\sqrt{2}q\hbar F}\right) \tag{2}$$

where m_r is the reduced mass of the conduction band effective mass m_c and the light hole effective mass m_{lh}, i.e., $1/m_r = 1/m_c + 1/m_{lh}$. E_g is the bandgap, q is the electron charge, and $\hbar$ is the reduced Planck's constant. F is the position-dependent electric field.

Trap-assisted tunneling is a complex process, with dependences on the position of trap inside the energy gap, the density of traps, trap occupation by electrons, and the trap potential. In recent modeling work, Donnelly *et al.* [5] set the tunneling current from the valence band to the trap equal to the tunneling current from the trap to the conduction band to determine the filling of the traps and obtain an explicit formula for the TAT current. By adopting this procedure, the dark carrier generation rate per unit volume due to TAT can be expressed as

$$N_{TAT} = \frac{\sqrt{\frac{2m_r}{E_g}}\frac{q^2F^2}{4\pi^3\hbar^2}N_{trap}\exp\left(-\frac{\pi\sqrt{m_{lh}E_{B1}^3}+\pi\sqrt{m_C E_{B2}^3}}{2\sqrt{2}q\hbar F}\right)}{N_V\exp\left(-\frac{\pi\sqrt{m_{lh}E_{B1}^3}}{2\sqrt{2}q\hbar F}\right)+N_C\exp\left(-\frac{\pi\sqrt{m_c E_{B2}^3}}{2\sqrt{2}q\hbar F}\right)} \tag{3}$$

where the barrier heights E_{B1} and E_{B2} govern tunneling from valence band-to-trap and trap-to-conduction band, respectively. N_v and N_c are the effective density of states for the valence and conduction bands, respectively, and N_{trap} is the trap concentration.

For calculating the breakdown voltage, a suitable model for ionization coefficients is required. Dead space effects have been found to play an important role in APDs with thin multiplication widths [17],[18]. However, for appropriately designed SPADs, multiplication widths are generally relatively thick, and it is reasonable to use a canonical local field model in which ionization coefficients depend on field only. We adopted the physical model of Zappa *et al*. [19], which takes into account the dependence of ionization coefficients on temperature. To calculate the count rate and detection efficiency, it is important to calculate the avalanche probability, and we adopted the model of McIntyre [20] for this purpose. The model of Adachi [21] was used for the calculation of absorption coefficient, and the effects of electroabsorption [22] and free carrier absorption have also been included.

For the parameters used in the calculation, the effective mass of electrons and holes, and the change of bandgap energy with temperature, were taken from [23]. Three important parameters—SRH lifetime τ_{SRH}, trap density N_{trap}, and trap energy level E_{trap}—are to be determined from the modeling. From fitting of our simulated results to the measured data, we find $\tau_{SRH} \sim 70$ µs. There have been past studies of the traps in InP [24]–[29] and $In_{0.53}Ga_{0.47}As$ [24], [25], [30]–[33], but there is no general agreement on the type, capture cross section, energy level, and concentration of traps in state-of-the-art epitaxially grown samples of these materials. Following Donnelly *et al.* [5], we define a parameter $\alpha = (E_{trap} - E_{v0})/E_g$ to identify the position of traps inside the energy bandgap, where E_{trap} is the energy level of trap and E_{v0} is the top of valence band. To derive appropriate parameters for quaternary alloys in the InGaAsP system, we use a linear

interpolation based on the energy bandgap of the alloy under consideration, with trap energy levels and concentrations in InP and $In_{0.53}Ga_{0.47}As$ taken as our reference materials. For the trap level in $In_{0.53}Ga_{0.47}As$, we adopted the value of [24], i.e., $\alpha(In_{0.53}Ga_{0.47}As) \sim 0.78$. For the trap level in InP, we adopted the value of [29], i.e., $\alpha(InP) \sim 0.75$. Based on fitting results, we find the following trap concentrations: $N_{trap}(In_{0.53}Ga_{0.47}As) \sim 1\times10^{15} cm^{-3}$ and $N_{trap}(InP) \sim 2\times10^{14} cm^{-3}$ for the 1.55 μm devices; and $N_{trap}(InP) \sim 4\times10^{14} cm^{-3}$ for our 1.06 μm SPADs.

4.2 Results of modeling

Using the formalism just described, we calculate both the DCR and the DE as a function of voltage overbias ΔV above the breakdown voltage V_{br}. Using DCR and DE values from successive ΔV, we can create the simulated curves for DCR vs. DE plotted in Figure 3 (solid lines) for operating temperatures of 230, 270, and 295 K. As pointed out at the end of Sub-section 3.1, the ΔV values used in the free-running measurements were lower than the values generally found in the more prevalent gated mode measurements for InP-based SPADs, and they are similarly lower than the modeled ΔV values for a given DCR or DE. However, as seen in Figure 3, the agreement with measured data for DCR vs. DE is excellent. In achieving these fits, we found the greatest sensitivity to the parameter α(InP) corresponding to the tunneling trap position within the InP bandgap. The fits for the three temperatures as shown in Figure 3 were accomplished for $\alpha(InP) = 0.75 \pm 0.02$.

In modeling DCR, all layers of the structure were considered. Figure 5 illustrates the calculated dependence on overbias ΔV of the total DCR as well as the contribution to DCR per unit area at 230 K and 295 K of the four principal layers of the SPAD structure, i.e., the multiplication, field control, grading, and absorption layers. Thermal and tunneling mechanisms described in Sub-section 4.1 were all considered for each layer. These layer-by-layer calculations show that the dominant contribution to DCR originates from either (i) trap-assisted tunneling (TAT) in the multiplication region or (ii) thermal generation in the absorption layer under all conditions considered (i.e., temperatures in the range 230 to 295 K, and overbias in the range 0 to 10 V). The relative importance of multiplication region TAT and absorption region thermal generation depends on the operating temperature and overbias. As seen in Figure 5(a), at 230 K, multiplication region TAT is at least an order of magnitude larger than contributions from all the other layers for ΔV > 0.2 V. In contrast, for 295K, Figure 5(b) illustrates that for ΔV less than 5 V, absorption layer thermal generation dominates; at higher voltages, multiplication region TAT becomes dominant.

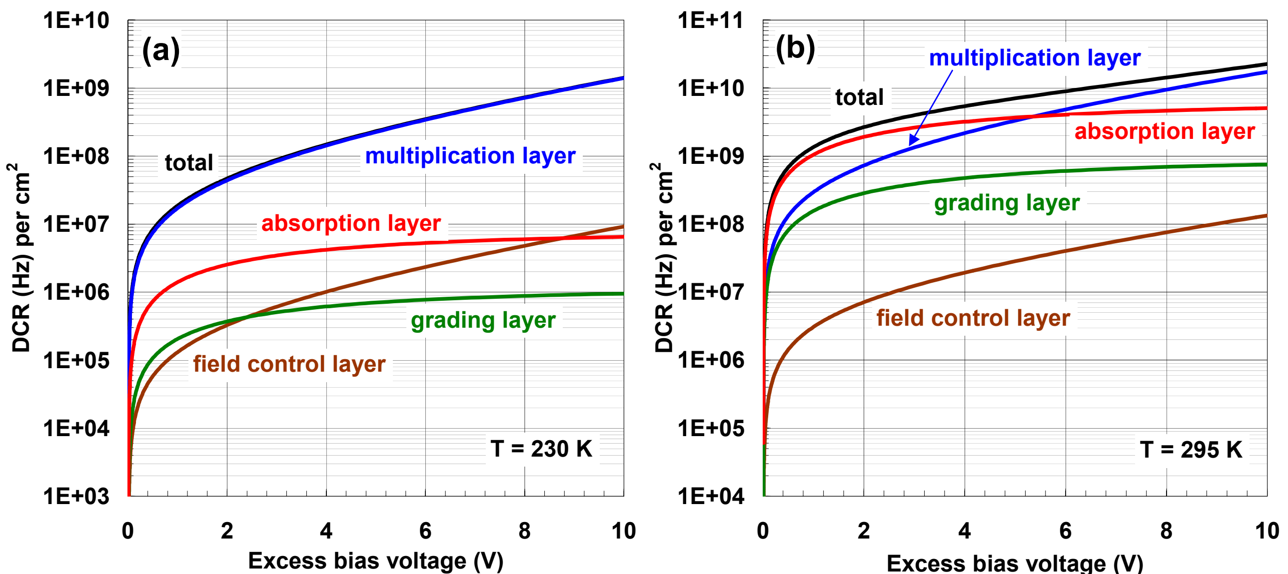

Figure 5. Calculated dependence of dark count rate (DCR) per cm^2 on overbias for InGaAsP/InP SPAD at (a) 230 K and (b) 295 K illustrated by curve labelled "total". Contribution to DCR of various layers is indicated, with dominant contributions seen from multiplication region trap-assisted tunneling and absorption region thermal generation. In (a), DCR from the multiplication layer dominates completely and is indistinguishable from the total DCR.

5. AFTERPULSING MEASUREMENTS

In a SPAD, the triggering of an avalanche event by a single photo-excited or dark-generated carrier results in the flow of a large number of impact-ionized carriers before the avalanche is quenched. The presence of defects in the multiplication region can lead to the trapping of at least a small fraction of these carriers. If the SPAD is quenched and re-armed before all of the trapped carriers have detrapped and escaped from the multiplication region, it is possible for detrapped carriers to seed subsequent avalanches. Counts initiated by detrapped carriers are referred to as "afterpulses" and will increase the overall dark count rate.

The most common technique for mitigating afterpulsing is the use of a "hold-off" time following the quenching of the SPAD during which the voltage bias is held below breakdown to prevent new avalanches from occuring while trapped carriers are detrapping. With a sufficiently long hold-off time, the probability of afterpulses occuring can be kept arbitrarily small. However, the use of longer hold-off times reduces the repetition rate at which counts can be obtained.

To characterize the afterpulsing in the 1.06 μm SPADs, we have obtained the afterpulse probability as a function of delay time using the autocorrelation of the dark count record from a multichannel scalar [34],[35]. Dark counts were measured using very short time bins (5 ns), which guarantees a negligible probability for two dark counts occuring within a single time bin. The data in Figure 6 show the probability that two time bins separated by a given delay time both contain dark counts. The presence of afterpulsing is indicated by the notable increase in the probability of dark count coincidence for shorter delay times. Data have been collected at 250 K at three different bias conditions corresponding to detection efficiencies of 1%, 8%, and 35%. For delay times shorter than ~1 μs, there is a dramatic increase in the afterpulse probability, especially for larger detection efficiencies. Strong afterpulsing effects for hold-off times shorter than ~1 – 10 μs are typical for InP-based SPADs utilizing InP multiplication regions [3].

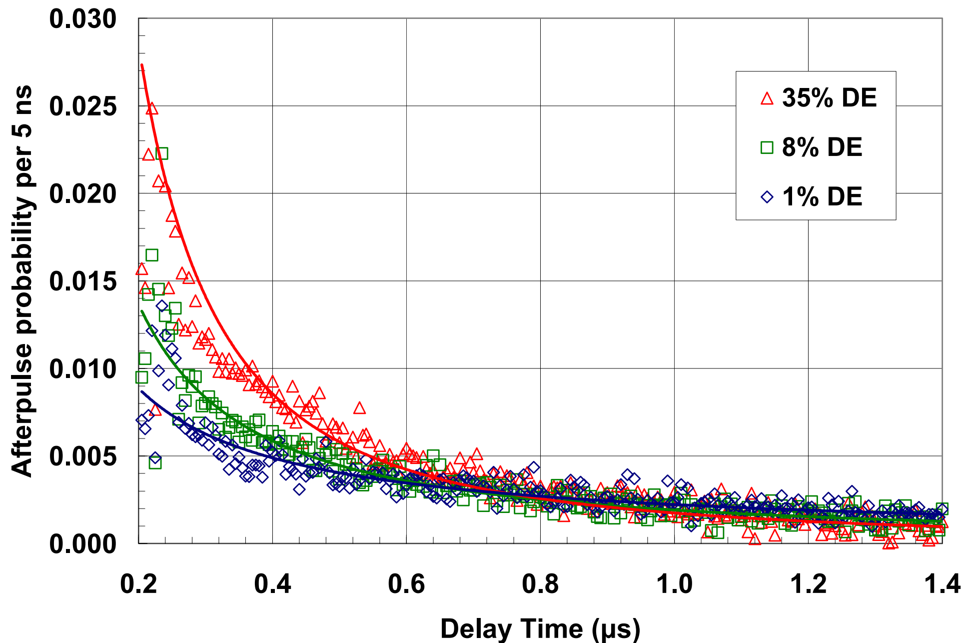

Figure 6. Afterpulsing probability extracted using dark count autocorrelation with 5 ns bins. Data were obtained at 250 K operation for voltage biases corresponding to detection efficiencies of 1%, 8%, and 35%. Solid lines are power-law approximations intended only to indicate trends in the three sets of data.

Aside from hold-off time, other operating conditions also influence the severity of afterpulsing effects. Because characteristic detrapping times decrease at higher temperatures, afterpulsing can be reduced by operating at higher temperature, but only at the expense of higher intrinsic dark count rates. Another factor that impacts afterpulsing is the total number of carriers that flow during an avalanche, since the number of trapped carriers will be proportional to this total number. Operation at lower overbias voltages generates smaller avalanches, and therefore less afterpulsing, but

also results in lower detection efficiencies. This trade-off between afterpulsing and detection efficiency is illustrated by the data in Figure 6, where lower afterpulsing coincides with lower detection efficiency. The use of monolithic arrays of SPADs [4] is also quite effective for reducing the impact of afterpulsing: even if one pixel is triggered and remains inoperative during the subsequent hold-off time, all other pixels in the array can remain armed. However, the readout electronics associated with the use of SPAD arrays are generally very complex. Finally, the most fundamental approach to reducing afterpulsing is through the reduction of defects that act as trap sites in the material of the multiplication region itself. To date, there has been no clear identification of the nature of these defects, and basic materials improvement poses a challenging, though potentially highly effective, approach to solving the problems of afterpulsing.

6. CONCLUSIONS

We have presented non-gated single photon counting measurements on InGaAsP/InP SPADs optimized for operation at 1.06 μm. Devices were characterized by measuring the total count rate as a function of photon flux for flux values in the range 10^{-1} to 10^{8} photons per second. Beyond a count rate of ~10^{4} s^{-1}, signal counts exceed dark counts. Signal counts can be measured over three orders of magnitude before saturation is encountered. At a detection efficiency of 10%, 80 μm diameter devices were shown to exhibit free-running operation with dark count rates below 1000 Hz when operated at 230 K. Under these conditions, photon counting rates exceeding 1 MHz have been obtained. Significantly higher detection efficiencies (>30%) are achievable with acceptable tradeoffs in dark count rate.

Modeling of fundamental 1.06 μm SPAD performance parameters, including dark count rate and detection efficiency, has been shown to be in excellent agreement with measurements of DCR vs DE for temperatures between ~230 and 300 K. Consideration of the individual dark carrier generation mechanisms shows that for our 1.06 μm SPADs, multiplication region tunneling dominates the DCR at lower temperatures on the order of 230 K, while both multiplication region tunneling and absorption region thermal generation are important at higher temperatures on the order of 295 K.

We have also shown similar experimental and modeling results obtained for longer cutoff wavelength InGaAs/InP SPADs designed for operation at telecom wavelengths on the order of 1.55 μm. At a given temperature and detection efficiency, these 1.55 μm SPADs exhibit a DCR two to three orders of magnitude larger than that of the 1.06 μm SPADs, and the dynamic range is greatly reduced—to less than one order of magnitude—at useful detection efficiencies (e.g., ≥10%).

Finally, initial characterization of afterpulsing effects in the 1.06 μm SPADs shows that afterpulsing effects are strong for hold-off times shorter than ~1 μs. To increase count rates beyond the range of 1 – 10 MHz, these afterpulsing characteristics will require improvements to allow for shorter hold-off times.

This work was supported by NASA under grant NNG06LA04C.

REFERENCES

[1] R. M. Measures, Laser Remote Sensing - Fundamentals and Applications, John Wiley & Sons (1984).
[2] Special Issue on "Free-space laser communications", IEEE LEOS Newsletter, vol. 19 No. 5 (2005).
[3] M.A. Itzler, R. Ben-Michael, C.-F. Hsu, K. Slomkowski, A. Tosi, S. Cova, F. Zappa, R. Ispasoiu, "Single photon avalanche diodes for 1.5 μm photon counting applications," J. Modern Optics, vol. 54, No. 2-3, in press (2007).
[4] K.A. McIntosh, J. P. Donnelly, D.C. Oakley, et al., "InGaAsP/InP avalanche photodiodes for photon counting at 1.06 μm," Appl. Phys. Lett., vol. 81 2505-2507 (2002).
[5] J. P. Donnelly, E. K. Duerr, K. A. McIntosh, et al., "Design Considerations for 1.06-μm InGaAsP-InP Geiger-Mode Avalanche Photodiodes," IEEE J. Quantum Electron., vol. 42, 797-809 (2006).
[6] K. Nishida, K. Taguchi, and Y. Matsumoto, "InGaAsP heterostructure avalanche photodiodes with high avalanche gain," *Appl. Phys. Lett.*, vol. 35, 251–252 (1979).
[7] J. C. Campbell, A. G. Dentai, W. S. Holden, and B. L. Kasper, "High-performance avalanche photodiode with separate absorption, 'grading', and multiplication regions, " *Electron. Lett.*, vol. 19, 818 – 820 (1983).
[8] S. R. Forrest, O. K. Kim, and R. G. Smith, "Optical response time of $In_{0.53}Ga_{0.47}As$ avalanche photodiodes," *Appl. Phys. Lett.*, vol. 41, 95–98 (1982).

[9] Y. Liu, S. R. Forrest, J. Hladky, M. J. Lange, G. H. Olsen, D. E. Ackley, *J. Lightwave Tech.,* vol. 10, 182 (1992).
[10] M. A. Itzler, C. S. Wang, S. McCoy, N. Codd, and N. Komaba, "Planar bulk-InP avalanche photodiode design for 2.5 and 10 Gb/s applications," *Proc. of 24th European Conference on Optical Communications (ECOC '98)*, vol. 1, 59 – 60 (1998).
[11] M. A. Itzler, K. K. Loi, S. McCoy, N. Codd, and N. Komaba, "Manufacturable planar bulk-InP avalanche photodiodes for 10 Gb/s applications, " *Proc. of 12th Annual Meeting of Lasers and Electro-Optics Society (LEOS '99)*, vol. 2, 748 – 749 (1999).
[12] M. A. Itzler, K. K. Loi, S. McCoy, N. Codd, and N. Komaba, "High-performance, manufacturable avalanche photodiodes for 10 Gb/s optical receivers, " *Proc. of 25th Optical Fiber Communication Conference (OFC 2000)*, vol. 4, 126 – 128 (2000).
[13] F. Zappa, A. Lotito, A.C. Giudice, S. Cova, and M. Ghioni, "Monolithic Active-Quenching and Active-Reset Circuit for Single-Photon Avalanche Detectors", IEEE J. of Solid-State Circuits, vol. 38, 1298-1301 (2003); see www.microphotondevices.com.
[14] D.S. Bethune, W.P. Risk, G.W. Pabst, "A high-performance integrated single-photon detector for telecom wavelengths", Journal of Modern Optics, vol. 51, no.9–10, pp. 1359–1368 (2004).
[15] R. Ben-Michael, M. A. Itzler, and B. Nyman, "Afterpulsing Effects in 1.5 µm Single Photon Avalanche Photodetectors," *2006 IEEE LEOS Annual Meeting Conference Proceedings* (LEOS '06), pp. 783–784 (2006).
[16] S.M. Sze, *Physics of Semiconductor Devices*. New York: Wiley, 1981, pp. 520-527.
[17] B.E.A. Saleh, M.M. Hayat, and M.C. Teich, "Effect of dead space on the excess noise factor and time response of avalanche photodiodes", *IEEE Trans. Electron Devices*, vol. ED-37, no. 9, pp. 1976-1984 (1990).
[18] R.J. McIntyre, "A new look at impact ionization-part I: a theory of gain, noise, breakdown probability, and frequency response", *IEEE Trans. Electron Devices*, vol. ED-46, no. 8, pp. 1623-1631 (1999).
[19] F. Zappa, P. Lovati and A. Lacaita, "Temperature dependence of electron and hole ionization coefficients in InP", in *Conf. Proc. Int. Conf. Indium Phosphide and Related materials (IPRM)*, pp. 628-631 (1996).
[20] R.J. McIntyre, "On the avalanche initiation probability of avalanche diodes above the breakdown voltage", *IEEE Trans. Electron Devices*, vol. ED-20, no. 7, pp. 637- 641 (1973).
[21] S. Adachi, "Optical dispersion relations for GaP, GaAs, GaSb, InP, InAs, InSb, $Al_xGa_{1-x}As$ and $In_{1-x}Ga_xAs_yP_{1-y}$", *J. Appl. Phys.*, vol. 66, no.12, pp. 6030-6040 (1989).
[22] R.H. Kingston, "Electroabsorption in GaInAsP", *Appl. Phys. Lett.*, vol. 34, no. 11, pp. 744-746 (1979).
[23] I. Vurgaftman, J.R. Meyer and L.R. Ram-Mohan, "Band parameters for III-V compound semiconductors and their alloys", *J. Appl. Phys.*, vol. 89, no. 11, pp. 5815 – 5875 (2001).
[24] S.R. Forrest and O.K. Kim, "Deep levels in $In_{0.53}Ga_{0.47}As$/InP heterostructures", *J. Appl. Phys.*, vol. 53, no. 8, pp. 5738–5745 (1982).
[25] F. Buchali, R. Behrendt and G. Heymann, "InGaAsP/InP-photodiodes with dark current limited by generation-recombination", *Electron. Lett.*, vol. 27, no. 3, pp. 235-237 (1991).
[26] J.M. Martin, S. Garcia, I. Martil, G. Gonzalez-Diaz, E. Castan, and S. Duenas, "Deep-level transient spectroscopy and electrical characterization of ion-implanted p-n junctions into undoped InP", *J. Appl. Phys*., vol. 78, no.9, pp. 5325-5330 (1995).
[27] T. Sugino, H. Ninomiya, T. Yamada, J. Shirafuji and K. Matsuda, "Creation and passivation of electron traps in n-InP treated with hydrogen plasma", *Appl. Phys. Lett.*, vol. 60, no. 10, pp. 1226-1228 (1992).
[28] S.H. Chiao and G.A. Antypas, "Photocapacitance effects of deep traps in n-type InP", *J. Appl. Phys.*, vol. 49, no. 1, pp. 466–468 (1978).
[29] O. Wada, A. Majerfeld and A.N.M.M. Choudhury, "Interaction of deep-level traps with the lowest and upper conduction minima in InP", *J. Appl. Phys.*, vol. 51, no. 1, pp. 423–432 (1980).
[30] G.J. Shaw, S.R. Messenger, R.J. Walters, and G.P. Summers, "Radiation-induced reverse dark currents in $In_{0.53}Ga_{0.47}As$ photodiodes", *J. Appl. Phys.*, vol. 73, no. 11, pp. 7244–7249 (1993).
[31] P. Philippe, P. Poulain, K. Kazmierski, and B. de Cremoux, "Dark-current and capacitance analysis of InGaAs/InP photodiodes grown by metalorganic chemical vapor deposition", *J. Appl. Phys.*, vol. 59, no. 5, pp. 1771–1773 (1986).
[32] K. Kazmierski, P. Philippe, P. Poulain, and B. de Cremoux, "C-V measurement and modelization of GaInAs/InP heterointerface with traps", *J. Appl. Phys.*, vol. 61, no. 5, pp. 1941–1946 (1987).
[33] Y. Takanashi and N. Kondo, "Deep trap in InGaAs grown by gas source molecular beam epitaxy", *J. Appl. Phys.*, vol. 85, no. 1, pp. 633–634 (1999).
[34] J. G. Rarity, T. E. Wall, K. D. Ridley, P. C. M. Owens, and P. R. Tapster, "Single-photon counting for the 1300–1600-nm range by use of Peltier-cooled and passively quenched InGaAs avalanche photodiodes," *Applied Optics*, vol. 39, pp. 6746–6753 (2000).
[35] M. A. Krainak, "Photoionization of Trapped Carriers in Avalanche Photodiodes to Reduce Afterpulsing During Geiger-Mode Photon Counting," *2005 Conf. on Lasers and Electro-Optics (CLEO)*, vol. 1, pp. 588-90 (2005).